

## Theory of photoemission from localized adsorbate levels\*

Ansgar Liebsch

Department of Physics, University of Pennsylvania, Philadelphia, Pennsylvania 19174

(Received 3 September 1975)

A detailed analysis of a recently developed theory of the angle- and energy-resolved photoemission from localized adsorbate levels is presented. The non-plane-wave nature of the final state originating in the repeated scattering of the outgoing wave by the surrounding atoms constitutes the essential feature of this theory. It is shown that the resulting interferences lead to experimentally observable structure in photoemission spectra which is sensitive to the position of the adsorbate relative to the substrate. Emphasis is placed on the emission from simple, atomiclike orbitals since they permit an unambiguous identification of final-state interactions. Sample calculations are performed to illustrate these effects in the case of emission from the adsorbate  $2s$  level for a sulfur monolayer on a nickel substrate.

### I. INTRODUCTION

The purpose of the present paper is to give a detailed analysis of a previously developed theory for the angle- and energy-resolved photoemission from localized adsorbate levels.<sup>1</sup> Final-state effects resulting from the multiple scattering of the photoemitted electron by the surrounding atomic environment represent the essential feature of this theory. Several aspects of the original model are extended. The theory is also applied to a realistic case, namely, a monolayer of sulfur adsorbed on a nickel substrate in order to demonstrate the dependence of calculated spectra on the geometrical structure of the overlayer relative to the substrate.

The motivation for this work is threefold: First, we would like to present a model that might contribute to a quantitative understanding of the photoemission process *per se*. Second, we would like to point out the potential of angle- and energy-resolved photoemission as a tool to determine geometrical structures at surfaces. In this regard, photoemission represents a technique complementary to low-energy electron diffraction (LEED), possibly more general in that it is not strictly limited to ordered overlayers or to relatively high coverages. Considering the great difficulties encountered in the theoretical description of almost any surface-sensitive experiment, the availability of two independent techniques measuring the same information is certainly highly desirable. As we will discuss in more detail below, the type of photoemission experiment that will be most suitable for this purpose is one that involves simple (i. e., localized nonbonding) initial states of adsorbed species and that utilizes appropriate photon energies such that the kinetic energy of the photoemitted electron lies in the range of typical LEED energies. Third, a quantitative understanding of final-state effects might enable one to extend the model to more complex initial states such as those resulting from the hybridization of substrate and

adsorbate wave functions. Gadzuk<sup>2</sup> has discussed this case for plane-wave final states and has pointed out that in this limit angular resolved photoemission directly probes the symmetry of bonding orbitals. Since such experiments promise to become a highly useful tool in the study of surfaces,<sup>3</sup> we regard the present work as a necessary first step toward their interpretation. By choosing the simplest possible initial state, we are able to focus attention on the details of the final state and thereby gain insight into this aspect of the problem. Once the validity of our final-state description is tested for a particular system in the case of emission from a simple initial state by comparing its predictions to corresponding LEED results, one could then attempt to interpret for the same system the emission intensities from orbitals involved in the bonding.

All of the existing angular resolved photoemission measurements on chemisorbed atoms and molecules<sup>4</sup> were performed on bonding-type orbitals. These initial states exhibit considerable angular anisotropies themselves, thus making the identification of final-state effects difficult. There is, however, a very close conceptual relationship to two other spectroscopies in which similar final-state effects are by now well established: the extended x-ray absorption fine structure (EXAFS) and angular-resolved Auger electron spectroscopy. The absorption coefficient in EXAFS,<sup>5</sup> as a function of the final electron energy, contains structure of the order of 10% of the mean signal that is characteristic of the geometry of the atomic environment near the atom which absorbs the photon. Since this coefficient differs from the photoemission current mainly in that it involves a summation over all final states, one would conclude that: (a) angular-integrated photoemission spectra also exhibit similar structure as function of final energy, i. e., that geometry effects are not entirely averaged out, and (b) that the final-state effects in angular distributions have to be considerably

more pronounced in order for the residual effects after angular integration to be of the same order as in EXAFS. In the case of Auger electron spectroscopy,<sup>6</sup> strong anisotropies have been observed as function of the detector direction. Although little is known about possible anisotropies originating in the excitation process of the Auger electron, most of the structure is thought to be due to the nature of the final state.<sup>6</sup> Thus the multiple scattering formalism described in this paper can also be applied to interpret the observed spectra in Auger electron spectroscopy.<sup>7</sup>

The emission from the localized core state is viewed in our model as a one-step process. The essential task lies in the evaluation of the single-particle propagator for the outgoing electron. Since our main interest is focused on the structural information contained in the excitation process, we make the following approximations: First, the potential in which the electron is moving is assumed to be time-independent and of muffin-tin form. The potential at the emitting site is taken to be that of an ionized atom with an additional electron inserted into the sulfur 4s shell to simulate the screening charge. Thus we ignore all many-body effects resulting from the interaction of the photoelectron with the hole left behind and from the time-dependent relaxation of the remaining electrons around the hole. Second, the spatial dependence of the vector potential<sup>8</sup> of the incoming light as well as explicit scattering of the outgoing wave by the smooth solid-vacuum barrier<sup>9</sup> is neglected. Although each of these approximations might not be valid in general, they become less severe as the photon energy and the kinetic energy increase, respectively.

The outgoing wave can be thought of as a superposition of two coherent contributions: a "direct" wave whose amplitude and symmetry is determined by the intra-atomic transition at the emitting site in the absence of any other potentials, and an "indirect" wave caused by the repeated scattering of the direct wave by the atomic environment. These scattering processes lead to structure in the photoemission spectra that is sensitive to the local atomic geometry near the emitting atom. Thus, one might view the emission from a localized orbital as a LEED problem with a "spherical" rather than a plane-wave source. In contrast to LEED, however, both the primary and the scattered waves are detected coherently. This simple argument permits a rough estimate of the size of the effects that are to be expected owing to the scattering. For a typical LEED reflectivity of 4%, the absolute value of the scattering amplitude is about 0.2; therefore, the leading correction to the direct photoemission intensity, namely, the cross term between the direct and indirect wave, would be of

the order of  $2 \times 0.2$  or 40%. Realistic calculations that we have performed for an ordered ( $1 \times 1$ ) layer of sulfur adsorbed on a (001) nickel surface confirm this estimate exhibiting in fact corrections up to 100%. We have chosen this particular system because it has been extensively studied by LEED.<sup>10</sup> The consideration of an ordered overlayer rather than a single adsorbed atom is based on the fact that the former corresponds more closely to the experimental situation and that the overall geometry is conceptually simpler. The ( $1 \times 1$ ) structure is chosen merely for computational ease. In order to calculate the indirect wave, we adapt the multiple scattering formalism employed in current LEED theories.<sup>11</sup> Electron-electron interactions that determine the short mean free path of the photoelectron are included by inserting a uniform complex self energy (optical potential) into the single-particle propagator.<sup>12</sup>

The question that is significant for practical purposes concerns the relative importance of single and multiple scattering of the outgoing wave. Multiple scattering effects contain information about the adsorption geometry in a rather convoluted form and therefore are not suitable for any simple Fourier-type analysis. In contrast to the model considered previously<sup>1</sup> (simple cubic crystal, s-wave scatterers), the results that we will describe below tend to indicate that the single scattering limit is generally not adequate and that multiple scattering events appear to be appreciable. Finite-temperature effects that are not included in the present calculations can be expected to reduce this importance to some extent. In this regard, the situation is comparable to LEED in that quantitative geometry information, e.g., the vertical spacing between overlayer and substrate, can only be extracted from experimental data by matching them with results obtained from full calculations. In addition, the various approximations concerning the spatial dependence of the vector potential, the details of the surface barrier, etc., could possibly limit one's ability to fit the data. As we will discuss further below, however, there are gross differences in the spectra even for adsorption sites of the same symmetry such as the top and center position. It remains to be investigated whether the dominant features of these spectra are sufficiently insensitive to some of the assumptions of our model that an identification with measured data is possible without too much computational effort.

The structure of the paper is as follows. In Sec. II, we discuss the formal procedure of evaluating the final state of the photoemitted electron. Only the essential steps are indicated; the detailed derivations of various results are presented in Appendices A-C. Section III contains the applica-

tion of the theory to a specific case, namely, that of a sulfur overlayer on a nickel substrate. Section IV summarizes our results and discusses some of their implications.

## II. FORMALISM

Let us assume that the adsorbed atom from which the electron is excited is located at the origin of the coordinate system and that the initial core-state wave function is defined by  $\Psi_i$ . In a one-electron description,<sup>13</sup> the wave function of the outgoing photoelectron at the position  $\vec{R}$  of the detector may be written

$$\Psi(\vec{R}) = \int d^3r G(\vec{R}, \vec{r}) \vec{p} \cdot \vec{A} \Psi_i(\vec{r}) \equiv G \vec{p} \cdot \vec{A} |\Psi_i\rangle, \quad (2.1)$$

where  $G$  is the final-state one-electron propagator describing the motion of the excited electron in the full potential due to substrate and overlayer. Equation (2.1) is based on the dipole approximation which can be regarded as adequate for low-photon energies ( $\hbar\omega \leq 10$  keV). As discussed in Sec. I, we ignore the spatial dependence of the vector potential  $\vec{A}$  and neglect explicit scattering of the outgoing electron from the smooth surface barrier. Thus, we first evaluate the above expression in the absence of any potential step. Subsequently, the actual angles of emission are determined by the usual refraction condition, namely, that the parallel component of the electron momentum is conserved across the solid-vacuum interface. The propagator  $G$  may formally be expressed in terms of the electron propagator  $G_0$  in the absence of the lattice potential and the  $T$  matrix of the entire system by using the Dyson equation

$$G = G_0 + G_0 T G_0. \quad (2.2)$$

$G_0$  contains a uniform complex self energy  $\Sigma$  (optical potential) whose real part  $V_0$  is the inner potential and whose imaginary part  $\Gamma$  accounts in a qualitative way for the strong inelastic electron-electron interactions. Since the outgoing electron also interacts with the potential due to the emitting atom, it is convenient to extract the corresponding single-site scattering vertex  $t_0$  from  $T$  and to consider all remaining scattering events separately

$$G = (1 + G_0 T') (G_0 + G_0 t_0 G_0). \quad (2.3)$$

This interaction with the central site was not included in the original model.<sup>1</sup> The remaining scattering matrix  $T'$  is defined as

$$T' = \sum_{\vec{R}_0 \neq 0} t_{\vec{R}_0} + \sum_{\vec{R}_1 \neq \vec{R}_0 \neq 0} i \vec{R}_1 G_0 t_{\vec{R}_0} + \dots, \quad (2.4)$$

i. e., the electron is allowed to return to the emitting site once it has been scattered by a lattice site  $\vec{R}_0 \neq 0$ . Using this decomposition of  $G$ , it becomes

obvious that  $\Psi$  involves two contributions

$$\Psi(\vec{R}) = \Psi^0(\vec{R}) + \Psi^1(\vec{R}). \quad (2.5)$$

The first represents the "atomic" part and is given by

$$\Psi^0(\vec{R}) \equiv (G_0 + G_0 t_0 G_0) \vec{p} \cdot \vec{A} |\Psi_i\rangle, \quad (2.6)$$

whereas the second accounts for the remaining part due to the presence of the surrounding atoms within the overlayer and the substrate,

$$\Psi^1(\vec{R}) \equiv G_0 T' |\Psi^0\rangle. \quad (2.7)$$

$\Psi^0$  is the analogous quantity that—in a one-electron description—determines the energy and angular dependence of the gas-phase photoionization cross section.<sup>14</sup> Thus, rather than calculating non-plane-wave corrections to the final state,<sup>1</sup> we consider it more appropriate to distinguish between the direct or "intra-atomic" contribution to the transition probability and the indirect contribution due to back scattering of the outgoing wave from the lattice, i. e., the "solid-state" corrections. The motivation for this distinction is twofold: On the one hand, it establishes a close conceptual relationship between photoemission spectra from adsorbates and corresponding experimental and theoretical gas phase results. On the other hand, it has the practical advantage of separating the part of the problem that depends essentially only on the potential of the surrounding atoms from other, more subtle aspects, which determine the intra-atomic transition. These include the change of the potential at the emitting site owing to the presence of the core hole and owing to its screening by the valence electrons. We also point out that possible orthogonality requirements of initial and final states only affect the intra-atomic matrix element since the spatial overlap of both states is limited to the muffin-tine sphere at the origin owing to the very short range of the initial core state. (It is not clear, however, to what extent such a requirement exists in the presence of a complex optical potential.<sup>15</sup>)

We now discuss a suitable representation for  $\Psi^0$ ; using this, we evaluate  $\Psi^1$ , first in the single scattering limit and subsequently for the case of multiple scattering.

The evaluation of the expression for  $\Psi^0$  proceeds by expanding the one-electron propagator  $G_0$  in terms of its partial wave components. The asymptotic limit for  $R \rightarrow \infty$  of the first term in Eq. (2.6) then simply leads to a plane-wave final state, thus making  $\Psi^0$  proportional to the Fourier transform of  $\Psi_i$ . The role of the second term representing the interaction of the outgoing wave with the emitting atom itself, however, is to replace the plane wave by a proper solution of the Schrödinger equation for the central site potential at the final electron energy. The details of this result are de-

rived in Appendix A. The final expression for  $\Psi^0(\vec{R})$ ,  $R \rightarrow \infty$ , has the following form:

$$\Psi^0(\vec{R}) \sim \frac{e^{i\kappa R}}{R} \sum_L Y_L^*(\hat{R}) M_{LL_i}(E_f, E_i), \quad (2.8)$$

$$M_{LL_i}(E_f, E_i) \sim \langle R_i Y_L | \vec{p} \cdot \vec{A} | \Psi_i \rangle. \quad (2.9)$$

Here,  $E_i$  and  $L_i$  denote the energy and quantum numbers ( $l, m$ ) of the initial level, respectively, and  $\kappa$  is the absolute value of the final electron momentum. The angular part of the matrix element  $M_{LL_i}$  selects the quantum numbers  $L$  that are allowed for a particular initial-state symmetry and orientation of the vector potential. These, in turn, define via the spherical harmonics  $Y_L(\hat{R})$ , the angular character of the emitted wave. ( $\hat{R}$  represents a unit vector in the direction of the detector.) The radial part of  $M_{LL_i}$  determines the dependence on the final electron energy which is seen to arise from the radial wave function  $R_l$ . The prefactor in Eq. (2.8) shows that  $\Psi^0$  has the proper asymptotic behavior of an outgoing wave.<sup>14</sup> The photoelectric current at the detector in the absence of scattering is therefore given by

$$j_0(E_f, E_i, \hat{R}) \sim \left| \sum_L Y_L^*(\hat{R}) M_{LL_i}(E_f, E_i) \right|^2. \quad (2.10)$$

In the single scattering limit, the correction term  $\Psi^1$  in Eq. (2.5) becomes

$$\Psi^1(\vec{R}) = G_0 \sum_{\vec{R}_0 \neq 0} t_{\vec{R}_0} | \Psi^0 \rangle. \quad (2.11)$$

Expanding both  $G_0$  and the single-site scattering vertex  $t_{\vec{R}_0}$  in terms of their angular momentum components, we obtain the following form for  $\Psi^1$  in the limit of  $R \rightarrow \infty$ :

$$\Psi^1(\vec{R}) \sim \frac{e^{i\kappa R}}{R} \sum_{LL'} Y_{L'}^*(\hat{R}) \times \left( \sum_{\vec{R}_0 \neq 0} e^{-i\vec{k} \cdot \vec{R}_0} t_{\vec{R}_0}^{\prime} G_{L',L}(\vec{R}_0) \right) M_{LL_i}(E_f, E_i), \quad (2.12)$$

where  $\vec{k}$  denotes the momentum of the outgoing electron. The derivation of this result is straightforward; it is presented, together with the definitions of  $t_{\vec{R}_0}^{\prime}$  and  $G_{L',L}$ , in Appendix B.

So far we have not made any assumptions regarding the geometrical structure of the adsorbed layer and that of the substrate. The evaluation of the multiple scattering contributions to  $\Psi^1$ , however, is simplified considerably if the overlayer shows the same symmetry as the substrate layers and if these layers are translationally invariant. The latter condition is satisfied with the exception of the emitting site whose potential is modified owing to the presence of the core hole. The former assumption is simply a matter of convenience and

the generalization to overlayers of lower symmetry than  $(1 \times 1)$  is straightforward. Thus we derive the multiple scattering contribution to  $\Psi^1$  for a set of arbitrarily stacked planes of atoms each of which exhibits translational invariance parallel to the surface. The correction due to the presence of the core hole is subsequently calculated explicitly in a perturbative method. The evaluation proceeds in three steps. The first involves the summation in Eq. (2.12) and in all higher-order contributions to  $\Psi^1$  over sites within individual planes of atoms. We specify these sites by two-dimensional vectors  $\vec{P}$  and denote the origin of the  $i$ th layer by  $\vec{d}_i$  (usually three dimensional). Because of the translational symmetry, the  $t$  matrices in Eq. (2.12) depend only on the layer index  $i$  (the overlayer has the index 0). Thus, the sums over  $\vec{P}$  naturally lead to the definition of the intra- and interplanar structure constants. The multiple scattering series involving sites is thereby reduced to a series involving atomic planes. In the second step, we sum over all multiple scattering events that take place within a given plane. These events form a geometric series and are conveniently expressed as a single-layer scattering matrix. The remaining multiple scattering series then contains sums over layer indices with the restriction that successive indices are unequal. In the final step, this series is written in terms of a multilayer scattering matrix which is defined via an algebraic system of equations. The correction to this series due to the perturbed potential at the emitting site constitutes a defect problem and has to be dealt with in a different manner. While elaborate methods exist that allow an exact treatment of this term, we will evaluate it below only to lowest order in the change of the  $t$  matrix at the origin.

Applying the above outlined procedure, we obtain the following expression for  $\Psi^1$ :

$$\Psi^1(\vec{R}) \sim \frac{e^{i\kappa R}}{R} \sum_{LL'} Y_{L'}^*(\hat{R}) \left( \sum_{i,j=0}^{\infty} e^{-i\vec{k}_i \cdot \vec{d}_i} T_{ij}(E_f, \vec{k}_{ii}) \times G_{j0}(E_f, \vec{k}_{ii}) + \Delta \right)_{L'L} M_{LL_i}(E_f, E_i). \quad (2.13)$$

The first term containing the multilayer scattering matrices  $T_{ij}$  and the structure constants  $G_{ij}$  represents the multiple scattering series in which the potential at the origin is replaced by its unperturbed version. The correction due to the actual potential is denoted by  $\Delta$ . The detailed definitions of these quantities, as well as the derivation of the above result, are also presented in Appendix B. The comparison of the expressions for  $\Psi^0$ , Eq. (2.8) and  $\Psi^1$ , Eq. (2.13), demonstrates in a rather plausible manner the physical mechanisms that give rise to the energy and angle dependence

of photoemission spectra. On the one hand, the energy distribution is influenced by two factors: (a) the intra-atomic transition probability given by  $M_{LL_i}$  and (b) the interferences due to back scattering of the outgoing wave from the neighboring atoms. The former quantity corresponds to the one that determines the energy dependence of the ionization cross section in gas-phase experiments. Thus, available theoretical methods in this area may be used to evaluate this quantity. The latter, however, depends exclusively on the potentials at the final energy and on the crystal structure, i.e., on the same set of parameters that are used in the interpretation of low-energy electron diffraction experiments (with the exception of the correction term  $\Delta$ ). Although in general it might not be easy to separate these two effects, data indicate<sup>16</sup> that the energy variation of  $M_{LL_i}$  is much smoother than that resulting from the interferences. On the other hand, the influence of the intra-atomic transitions on the angular dependence is very much simpler since it is given directly by the symmetry of the initial state and the direction of the vector potential. For example, initial states with  $l_i \neq 0$  can couple into two channels  $l_i \pm 1$  whose relative weights  $M_{l_i \pm 1, l_i}$  and  $M_{l_i - 1, l_i}$ , however, are independent of the exit angle. In Sec. III, we consider in detail the emission from an  $s$  orbital ( $l_i = 0$ ). The outgoing atomic wave then has  $p$  character ( $l_i + 1 = 1$ ), and the remaining structure in the angular distribution originates entirely in the interferences due to back scattering. Only in this case has the enhancement factor, i.e., the ratio of the actual emission current  $j$  and the current  $j_0$  in the absence of scattering, a particular simple form since the intra-atomic matrix element can be divided out:

$$\frac{j(E_f, E_i, \vec{R})}{j_0(E_f, E_i, \vec{R})} = \left| Y_L^*(\hat{R}) + \sum_{L'} Y_{L'}^*(\hat{R}) F_{L'L}(E_f, \vec{k}_i) \right|^2 / |Y_L^*(\hat{R})|^2, \quad (2.14)$$

where  $F_{L'L}$  is defined as the expression in the large parentheses of Eq. (2.13) and  $L = (l, m)$  now denotes the quantum numbers of the outgoing atomic wave.<sup>5</sup> It is this enhancement factor that we are exclusively concerned with in our calculations below. Since it does not depend on the matrix element  $M_{LL_i}$ , this case is most useful to study the effect of final-state interactions on photoemission spectra.

### III. RESULTS AND INTERPRETATIONS

We now apply the results derived in Sec. II to the case of photoemission from an ordered  $(1 \times 1)$  overlayer of sulfur adsorbed on the (001) face of a nickel substrate. More specifically, we con-

sider the excitation from the atomiclike  $2s$  orbital of one of the S atoms, i.e.,  $L_i = (0, 0)$ , whose energy is approximately 220 eV below the vacuum. As discussed in Sec. II, an  $s$  orbital permits the clearest identification of final-state effects. The radiation is assumed to be  $p$  polarized with the angle of incidence at grazing, i.e., the vector potential  $\vec{A}$  points along the surface normal which is taken to be the  $z$  direction of our coordinate system. The selection rules then limit the sum over  $L$  in Eqs. (2.8) and (2.13) to a single  $p$ -type state, namely,  $L = (1, 0)$ . The transition probability consequently is proportional to the intra-atomic matrix element  $M_{ps}(E_f, E_i)$ , and the remaining factor consists of two contributions, one representing the angular distribution of the direct wave and the other the energy- and angle-dependent distribution of the indirect wave. These two contributions are indicated schematically in Fig. 1. Although accurate potentials will ultimately represent a crucial ingredient in the theoretical interpretation of data, the calculations that we describe in this section are performed using four phase shifts determined from nonoverlapping atomic potentials. We feel, however, that this approximation is adequate at this stage since our main purpose is to demonstrate the nature of the final state and not to give precise intensity predictions. For the same reason, the multiple scattering calculations are carried out in a scheme analogous to the so-called renormalized forward scattering method proposed by Pendry.<sup>17</sup> In this scheme, relatively weaker backward scattering events are included to first order whereas forward scattering events (as well as multiple scattering within atomic planes) are treated exactly. In LEED this method represents an adequate description of the exact result for final energies above 10 eV.<sup>17</sup> In order to reduce

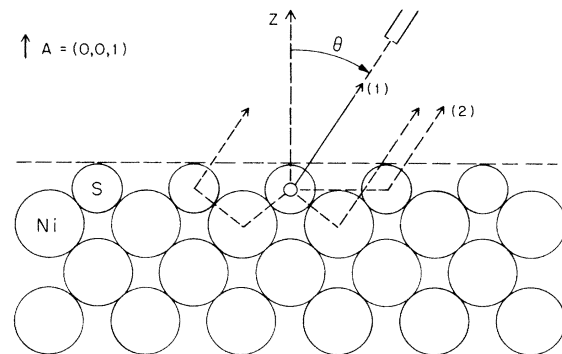


FIG. 1. Illustration of two processes contributing to photoemission from a localized adsorbate  $s$  orbital: (i) direct emission into atomic  $p$ -type final state and (ii) indirect emission via backscattering of the direct wave from the surrounding atoms. Only two single and one multiple scattering event are indicated.

the number of parameters of our model, we assume the inner potential  $V_0$  to be constant throughout the substrate and overlayer, at a value of 16 eV. This is not a realistic approximation since a change of  $V_0$  from substrate to overlayer leads to similar effects on the intensity distributions as a variation in the overlayer-substrate separation. An improvement upon this assumption is, however, easily achieved in ways analogous to those used in present LEED calculations.<sup>18</sup> Finally, the electronic damping is taken to be proportional to the "line of sight," i. e., spatially isotropic with a mean free path  $\lambda_{ee}$  (amplitude attenuation coefficient) of 8 Å, similar to that employed in recent interpretations of LEED spectra from S on Ni.<sup>10</sup>

#### A. Single scattering

In order to facilitate the analysis of final-state effects, we discuss first in greater detail the single scattering limit, since this allows us to gain a better understanding of the results obtained above and to study their implications. For this purpose it is convenient to bring the single scattering formula given in Eq. (2.12) into a slightly different form. Inserting into the lowest-order term in Eq. (2.13) the expression for the off-diagonal structure constants given in Eq. (B10) of Appendix B, the sum over substrate planes  $i=1, 2, \dots$ , reduces to a geometric series, and we obtain the following result for the enhancement factor of the photoemission current due to back scattering:

$$\begin{aligned} \frac{j}{j_0} = & \cos^{-2} \theta \left| \cos \theta + \sqrt{\frac{4}{3}} \pi \sum_{L'} Y_{L'}^*(\hat{R}) \sum_{\vec{P} \neq 0} e^{-i\vec{k} \cdot \vec{P}} t_0'(\kappa) \right. \\ & \times G_{L'L}(\vec{P}) - \frac{1}{2i\kappa A} \sum_{\vec{g}} t_1(\vec{k}, \vec{K}_g^-) \\ & \left. \times \frac{e^{i\vec{g} \cdot \vec{d}'_0} e^{i[\kappa(0) + \kappa(\vec{g})] |d'_1|}}{1 - e^{i\vec{g} \cdot \vec{d}'_0} e^{i[\kappa(0) + \kappa(\vec{g})] |d_1|}} \right|^2. \end{aligned} \quad (3.1)$$

Here,  $\vec{d}' = \vec{d}'_1 - \vec{d}_0$  and  $\vec{d} = \vec{d}_2 - \vec{d}_1$  denote the relative separation between overlayer and substrate and between successive substrate planes, respectively,

$$\kappa(\vec{g}) = [(2m/\hbar^2)(E_f + V_0 + i\Gamma) - (\vec{k}_{||} + \vec{g})^2]^{1/2}$$

and

$$\vec{K}_g^- = (\vec{k}_{||} + \vec{g}, -\kappa(\vec{g})).$$

The  $\vec{g}$ 's are the reciprocal-lattice vectors of the planes parallel to the surface,  $A$  is the area of the unity cell, and

$$t_1(\vec{k}, \vec{K}_g^-) = \sum_L Y_L^*(\hat{h}) t_1'(\kappa) Y_L(\hat{K}_g^-) \quad (3.2)$$

is the Fourier transform of the  $t$  matrix of the substrate atoms. The individual terms appearing in the expression for  $j/j_0$  represent, respectively, no scattering, single scattering from the overlayer atoms, and single scattering from all substrate

atoms.

The term describing single scattering from the substrate consists of a superposition of "beams" defined by  $\vec{g}$  each of which exhibits the following features: (a) The denominator leads to maxima whose physical origin lies in the constructive interference of waves that are scattered by successive substrate planes. These maxima are therefore characteristic of the substrate geometry only. The condition for them to occur is given by

$$\text{Re}\{\vec{g} \cdot \vec{d}'_0 + [\kappa(0) + \kappa(\vec{g})] |d_1|\} = 2\pi n, \quad (3.3)$$

$n$  integer. It can easily be shown that these conditions are related to certain features of the corresponding free-electron band structure of the solid. (b) The adsorption geometry enters the expression only via two phase factors: one for the normal position  $d'_1$  and one for the parallel displacement  $\vec{d}'_0$  of the overlayer relative to the substrate. (c) The individual beams are proportional to the  $t$  matrix of the substrate atoms, evaluated on the energy shell and for scattering angles that are related by reciprocal-lattice vectors  $\vec{g}$ . ( $\vec{k}$  points out of the crystal toward the detector, whereas  $\vec{K}_g^-$  is directed into the crystal.) Owing to the fact that the  $t$  matrix and the two phase factors are complex quantities, the maxima caused by the denominator can effectively be shifted by rather substantial amounts. Thus it becomes evident that the substrate potentials have to be known accurately if the overlayer geometry is to be determined.

In order to illustrate some of these features, we show in Fig. 2 the enhancement factor  $j/j_0$ , Eq. (3.1) as a function of final energy for emission along the surface normal. Curves (a)–(c) demonstrate the influence of the adsorption geometry. By choosing an energy independent  $\frac{1}{2}\pi$  s-wave potential, we are able to focus on this aspect alone and the curves show how the intensity peaks are shifted if the vertical separation between overlayer and substrate is varied. In the case that the spacing equals that between substrate planes [curve (b)], the maxima are seen to coincide with certain band crossings in the free-electron band structure indicated at the top of the figure. In panel (d), we illustrate the effect of the  $t$  matrix by comparing curve (b) with the corresponding intensity obtained for the actual substrate potential.

The term describing single scattering from the overlayer, i. e., the second term in Eq. (3.1) reflects only the geometry and potential of the overlayer itself. For the  $(1 \times 1)$  structure that we consider here, the intensity along the surface normal is shown in Fig. 3(a) (dashed curve). Additional peaks would occur in this spectrum for overlayers with lower symmetry due to new reciprocal-lattice vectors.

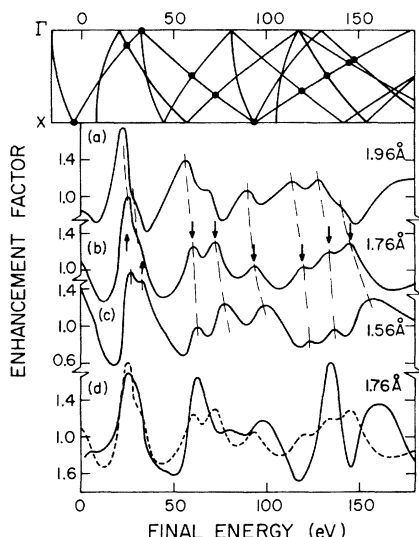


FIG. 2. Enhancement factor, Eq. (2.14), as a function of final energy for emission along the surface normal. (a)–(c) single scattering from substrate  $\frac{1}{2}\pi$  s-wave potentials for adsorption in center position at three vertical spacings. (d) single scattering from substrate Ni potentials (solid line) and  $\frac{1}{2}\pi$  s-wave scatterers (dashed line) for geometry as in (b). The arrows indicate the conditions for maxima Eq. (3,3), that coincide with band crossings in the free-electron band structure at the top of the figure.

### B. Multiple scattering

In the remainder of this section we present the results of various multiple scattering calculations. The emphasis is placed upon the comparison of energy and angle distributions for two separate overlayer geometries, one in which the sulfur atoms are adsorbed in the center position between nickel atoms and the other in which they are adsorbed on top. The vertical spacing between overlayer and the first substrate plane is in each case determined by the condition of touching atomic spheres, i. e.,  $\vec{d}' = (a/2\sqrt{2}, a/2\sqrt{2}, 1.4 \text{ \AA})$  and  $\vec{d}' = (0, 0, 2.245 \text{ \AA})$ , respectively, where  $a = 3.52 \text{ \AA}$  is the lattice constant of Ni.

In Fig. 3 we show the enhancement factor as a function of final energy for emission along the surface normal. The curves represent the results for multiple (solid lines) and single scattering (dashed lines). Panels (a) and (b) indicate, respectively, the contribution due to scattering from the overlayer and from the substrate to the intensity for the center position shown in panel (c). We point out that to lowest order in the scattering factors, these two contributions enter the total intensity additively because of the coherent detection of the direct and indirect wave. The comparison of panels (b) and (c) shows that the scattering from the substrate dominates the entire spectrum

with the exception of the structure below 10 eV. Panel (d) indicates the enhancement factor for the case of adsorption in the top position. Although some similarities do exist between the single and multiple scattering results, the agreement is generally not sufficient for the single scattering limit to be adequate.

The above calculations are performed for a translationally invariant overlayer in which the actual potential at the emitting site is replaced by an unperturbed sulfur potential. In order to estimate the influence of the ionized atom, we have calculated the correction term  $\Delta$  in Eq. (2.23) to lowest order in  $\delta t_0$ . The necessary phase shifts were determined for a sulfur atom in which the 2s shell is singly occupied and in which an additional electron in the 4s shell simulates the screening charge. The resulting changes in the intensity due to this correction turned out to be less than 5%.

It is apparent from Eq. (3.3) and the definition of  $\kappa(\vec{g})$  that for  $\vec{k}_i = 0$ , i. e., emission along the surface normal, the energies at which maxima in the single scattering spectra occur are degenerate with regard to various vectors  $\vec{g}$  whose components have opposite signs. At finite exit angles, however, these degeneracies split rapidly (analogous to the behavior of energy bands away from symmetry lines) thus leading to strong angular depen-

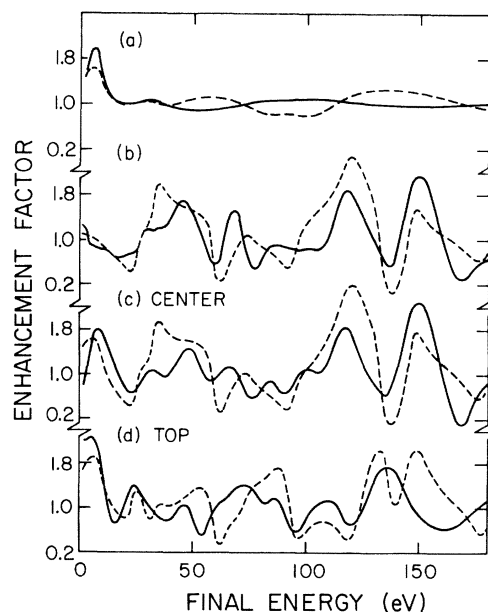


FIG. 3. Enhancement factor as a function of final energy for emission along the surface normal for multiple (solid lines) and single scattering (dashed lines). (a)–(c) scattering from overlayer, from substrate, and from entire system for adsorption in center position. (d) scattering from entire system for adsorption in top position.

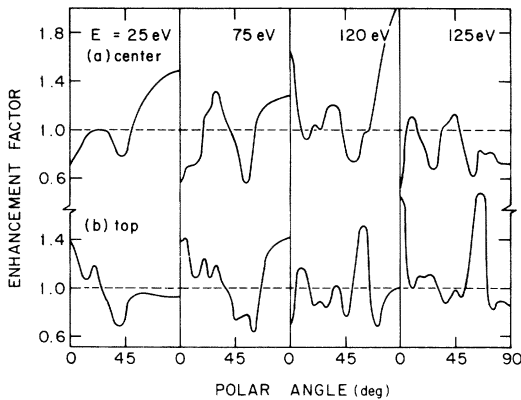


FIG. 4. Enhancement factor (multiple scattering) as a function of polar angle for various final energies at a fixed azimuth  $\Phi = 0$ . (a) overlayer adsorbed in center position and (b) in top position.

dence of the emission intensity. This structure is expected to be even richer in the multiple scattering limit owing to additional allowed interferences. In Fig. 4 we show the enhancement factor as function of polar angle for various final energies and a fixed azimuthal angle  $\Phi = 0$  (the  $x$  axis points along the direction of nearest neighbors within the surface plane). According to the first term in Eq. (3.1), the intensity in the absence of final-state effects would be proportional to  $\cos^2\theta$ . Panels (a) and (b) illustrate the distributions for the center and top position, respectively. We point out that the patterns change rather dramatically with final energy and exhibit marked differences for the two geometries. The corresponding single scattering results, not shown here for clarity, tend to follow the overall behavior of these patterns; nevertheless, considerable differences with regard to details do exist.

Finally, in Fig. 5 the azimuthal dependence of the enhancement factor is demonstrated for various energies and polar angles. Again, there are rapid variations in the angular distribution and the two geometries [panels (a) and (b)] lead to rather distinct patterns.

The calculations described in this section are performed for a sharp initial level. It is interesting to study how the final state influences the observed shape of a level that has a finite intrinsic width. In Ref. 19 such effects are discussed for the model considered previously.<sup>1</sup> The results show that the line shape can depend sensitively on the energy of the photoelectron and the detector direction. These modifications may in fact be so strong as to cause an apparent shift of the peak position.

#### IV. CONCLUSION

The results presented in Sec. III indicate that the final state in the case of photoemission from

localized adsorbate levels can deviate appreciably from a simple plane wave. This modification originates in the scattering of the outgoing wave by the surrounding atoms. We have shown that these interferences lead to structure in the energy and angle distributions that is characteristic of the local atomic geometry in the vicinity of the emitting atom. The same physical mechanism gives rise to the fine structure observed in extended x-ray adsorption fine structure (EXAFS). In contrast to EXAFS, however, which is performed as an absorption experiment, photoemission is highly surface sensitive because of the short electron escape depth. Thus one possible utilization of the photoemission lies in the determination of adsorption sites. The increased availability of continuous light sources in conjunction with the use of high-resolution angular analyzers represents an important step in the realization of this application. The calculations for S on Ni discussed above indicate that a quantitative interpretation of experimental spectra requires (a) accurate atomic potentials and (b) the inclusion of multiple scattering effects, i.e., the same ingredients necessary for the interpretation of LEED data. In addition the photoemission process involves several features such as the spatial dependence of the vector potential and the presence of the core hole, which could complicate the interpretation. As some of these effects are so far inaccessible to a detailed theoretical treatment, it is not known at the present moment how important they ultimately will be.

As we have also shown qualitatively different adsorption sites, e.g., the top and center position, lead to markedly different angle and energy distributions despite the fact that both exhibit four-fold symmetry. If the main features of these spec-

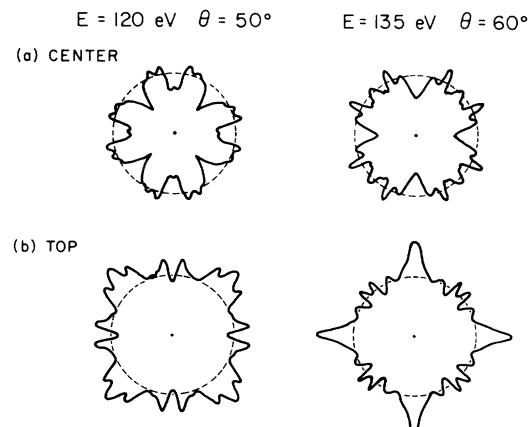


FIG. 5. Enhancement factor (multiple scattering) as a function of azimuthal angle for various final energies and polar angles. (a) overlayer adsorbed in center position and (b) in top position.

tra do not depend strongly on the approximations of our model, it will be possible to identify such positions without too much computational effort. Further investigations in this area are needed.

Our main interest in the present work was focused on the emission from localized  $s$  orbitals since they allow a clear isolation of final-state effects. We have found these effects to be large throughout the entire energy range considered. With regard to experiments performed on levels in the bonding region, the above results indicate that great caution is required in ascribing all observed structures exclusively to the initial state. We do not mean to imply that the final state dominates the spectra; it may in fact well be the case that some initial-state features like wave-function nodes, etc., have a greater influence than any occurring final-state interactions. In general, the matrix element describing the electronic transition involves both states in a intimately connected form; *to disentangle them, if at all possible, requires a careful analysis.* It is hoped, however, that a better understanding of the final state obtained through the consideration of simple initial states enables one to extend the theory to bonding-type orbitals whose study has become of great interest in the area of surface physics.

#### ACKNOWLEDGMENTS

It is a pleasure to thank Professor T. Gustafsson, Professor E. W. Plummer, Professor P. Soven, and Professor J. R. Schrieffer for many helpful and stimulating discussions. I am also grateful to Dr. C. B. Duke for the opportunity to use parts of his LEED computer program.

#### APPENDIX A

This appendix contains the derivation of the expressions for  $\Psi^0$  given in Eqs. (2.8) and (2.9). The major uncertainty in the evaluation of the intra-atomic matrix element lies (a) in the actual form of the  $t$  matrix  $t_0$  in Eq. (2.6), i.e., in the potential that the emitted electron interacts with at the origin, and (b) the role of electronic damping during this interaction. For simplicity we assume here that the remaining electrons are unrelaxed (i.e., Koopmans's theorem applies) and that damping can be ignored (this corresponds to the use of phase shifts calculated at real energies). In this case, the potential is the same for both initial and final state, so that the two are orthogonal.

The propagator  $G_0$  has the following expansion in terms of spherical coordinates:

$$G_0(\vec{r} - \vec{r}') = \sum_L Y_L^*(\hat{r}) G_L(r, r') Y_L(\hat{r}'), \quad (\text{A1})$$

$$G_L(r, r') = -ik h_i^{(1)}(\kappa r_{>}) j_i(\kappa r_{<}), \quad (\text{A2})$$

where  $r_{>}$  ( $r_{<}$ ) is the larger (smaller) value of  $r$  and  $r'$  and  $\kappa = [(2m/\hbar^2)(E_f + V_0)]^{1/2}$ . The  $Y_L$ ,  $j_i$ , and  $h_i^{(1)}$  are, respectively, complex spherical harmonics, spherical Bessel functions, and spherical Hankel function of the first kind. Writing the vertex  $t_0$  in Eq. (2.6) in terms of the spherically symmetric potential  $v(r)$  at the origin, we obtain for  $\Psi^0$

$$\begin{aligned} \Psi^0(\vec{R}) = & \sum_L Y_L^*(\hat{R}) (-ik h_i^{(1)}(\kappa R) \int d^3r \\ & \times \left( j_i(\kappa r) + \int dr' r'^2 j_i(\kappa r') v(r') G_L(r', r) + \dots \right) \\ & \times Y_L(\hat{r}) \vec{p} \cdot \vec{A} \Psi_i(\hat{r}). \end{aligned} \quad (\text{A3})$$

It is easily shown that the expression in the large parentheses is equivalent to the radial wave function  $R_l(\kappa r)$  multiplied by  $\exp(i\delta_0^l)$  where  $\delta_0^l$  is the  $l$ th partial-wave phase shift of the potential at the origin. This prefactor merely ensures that  $R_l$  has the correct asymptotic behavior, namely,

$$R_l(\kappa r) \rightarrow \cos \delta_0^l j_l(\kappa r) - \sin \delta_0^l n_l(\kappa r), \quad r \rightarrow \infty.$$

Using the asymptotic form for  $h_i^{(1)}$ ,

$$h_i^{(1)}(\kappa R) \rightarrow (-i)^i e^{i\kappa R}/i\kappa R, \quad R \rightarrow \infty, \quad (\text{A4})$$

we obtain the following result for  $\Psi^0$  at the position of the detector:

$$\Psi^0(\vec{R}) \rightarrow \frac{e^{i\kappa R}}{R} \sum_L Y_L^*(\hat{R}) M_{LL_i}(E_f, E_i), \quad (\text{A5})$$

$$M_{LL_i}(E_f, E_i) = -(-i)^i e^{i\delta_0^l} \langle R_L Y_L | \vec{p} \cdot \vec{A} | \Psi_i \rangle, \quad (\text{A6})$$

where  $E_i$  and  $L_i$  denote the energy and the angular quantum numbers of the initial level, respectively.

#### APPENDIX B

In this appendix, we first derive the single scattering expression for  $\Psi^1$ , Eq. (2.12), and subsequently discuss its extension to the multiple scattering limit, Eq. (2.13). The formalism is similar although not identical to that due to Beeby.<sup>20</sup>

Equations (A1) and (A2) of Appendix A lead to the identity

$$\begin{aligned} j_i^{-1}(\kappa r'') \int d\Omega_{r''} G_0(\vec{r}' - \vec{r}'') Y_L^*(\hat{r}'') \\ = -ik h_i^{(1)}(\kappa r') Y_L(\hat{r}') \end{aligned} \quad (\text{B1})$$

for  $r'' < r'$ . Substituting this in Eq. (A3),  $\Psi^0$  may be written

$$\begin{aligned} \Psi^0(\vec{r}') = - \sum_L i^i j_i^{-1}(\kappa r'') \int d\Omega_{r''} \\ \times G_0(\vec{r} - \vec{r}'') Y_L^*(\hat{r}'') M_{LL_i}. \end{aligned} \quad (\text{B2})$$

Inserting this form into the explicit version of Eq.

(2.11) and taking the asymptotic limit  $R \rightarrow \infty$  for  $G_0$ , we obtain for  $\Psi^1$

$$\begin{aligned} \Psi^1(\vec{R}) &= \frac{e^{i\kappa R}}{4\pi R} \sum_{\vec{R}_0 \neq 0} \int d^3r \int d^3r' e^{-i\vec{k} \cdot \vec{r}} \\ &\times t_{\vec{R}_0}(\vec{r} - \vec{R}_0, \vec{r}' - \vec{R}_0) \sum_i i^l j_l^{-1}(\kappa r') \\ &\times \int d\Omega_{r'} G_0(\vec{r}' - \vec{r}'') Y_L^*(\hat{r}'') M_{LL_i}, \end{aligned}$$

where  $\vec{k}$  is the momentum of the outgoing electron, i. e.,  $|\vec{k}| = \kappa$  and  $\hat{k} = \hat{R}$ . The condition  $r'' < r'$  is indeed satisfied since the initial-state wave function is assumed to be confined to the muffin-tin sphere at the origin. We now change variables from  $\vec{r}$  and  $\vec{r}'$  to  $\vec{r} + \vec{R}_0$  and  $\vec{r}' + \vec{R}_0$  and expand  $\exp(-i\vec{k} \cdot \vec{r})$  and  $t_{\vec{R}_0}(r, r')$  in terms of spherical harmonics. If we then define quantities

$$t_{\vec{R}_0}^i(\kappa) = \int d r r^2 \int d r' r'^2 j_l(\kappa r) t_{\vec{R}_0}^i(r, r') j_l(\kappa r'), \quad (\text{B3})$$

$$\begin{aligned} G_{LL'}(\vec{R}_0) &= \frac{(-i)^{l-l'}}{j_l(\kappa r) j_{l'}(\kappa r')} \int d\Omega_r \int d\Omega_{r'} Y_L(\hat{r}) \\ &\times G_0(\vec{r} + \vec{R}_0 - \vec{r}') Y_{L'}^*(r'), \quad (\text{B4}) \end{aligned}$$

we arrive at the following result for  $\Psi^1$  [see Eq. (2.12)]:

$$\begin{aligned} \Psi^1(\vec{R}) &= \frac{e^{i\kappa R}}{R} \sum_{LL'} Y_{L'}^*(\hat{R}) \\ &\times \left( \sum_{\vec{R}_0 \neq 0} e^{-i\vec{k} \cdot \vec{R}_0} t_{\vec{R}_0}^i(\kappa) G_{LL'}(\vec{R}_0) \right) M_{LL_i}. \quad (\text{B5}) \end{aligned}$$

The  $t_{\vec{R}_0}^i$  are related to the phase shifts  $\delta_{\vec{R}_0}^i$  in the usual way:

$$t_{\vec{R}_0}^i(\kappa) = (-1/2i\kappa) (e^{2i\delta_{\vec{R}_0}^i} - 1), \quad (\text{B6})$$

and the  $G_{LL'}$  may be written

$$\begin{aligned} G_{LL'}(\vec{R}_0) &= -i\kappa 4\pi \sum_{L''} (-i)^{l''} I(L; L'', L') \\ &\times h_{l''}^{(1)}(\kappa R_0) Y_{L''}(-\hat{R}_0), \quad (\text{B7}) \end{aligned}$$

where the  $I(L; L'', L')$  denote the Gaunt coefficients.

In order to evaluate  $\Psi^1$  in the multiple scattering limit, we now decompose the sum over  $\vec{R}_0$  in Eq. (B5) into a sum over layer indices  $i$  and over sites  $\vec{P}$  within planes. Because of the translational invariance parallel to the surface (we discuss the correction due to the core hole further below), the  $t$  matrices only depend on  $i$  and the sum over  $\vec{P}$  leads to the definition of the structure constants. It is convenient to introduce the following matrices:

$$t_i(\kappa) = \left| \left| t_i^i(\kappa) \delta_{LL'} \right| \right|, \quad (\text{B8})$$

$$G_{ij}(E_f, \vec{k}_0) = \left| \left| \sum_{\vec{P}}' e^{-i\vec{k}_0 \cdot (\vec{P} + \vec{d}_i - \vec{d}_j)} G_{LL'}(\vec{P} + \vec{d}_i - \vec{d}_j) \right| \right|. \quad (\text{B9})$$

The prime indicates that the term  $\vec{P} = 0$  is to be excluded from the sum in the case of the intraplanar structure constants ( $i = j$ ). In the presence of damping, the sums over  $\vec{P}$  converge rapidly for  $i = j$  and  $i \neq j$ . In the low-energy region, the off-diagonal structure constants ( $i \neq j$ ) may be computed more efficiently by performing in Eqs. (B9) and (B4) first the sum over sites  $\vec{P}$  which leads to a highly convergent sum over reciprocal-lattice vectors  $\vec{g}$  of the surface Bravais net

$$\begin{aligned} G_{ij}(E_f, \vec{k}_0) &= \left| \left| \sum_{\vec{g}} \frac{8\pi^2}{A i \kappa(\vec{g})} Y_L(\hat{K}_g^\pm) Y_{L'}^*(\hat{K}_g^\pm) \right. \right. \\ &\times \exp[i\vec{g} \cdot (\vec{d}_i - \vec{d}_j) + i\kappa(\vec{g}) |d_{i\perp} - d_{j\perp}|] \left. \left. \right| \right|. \quad (\text{B10}) \end{aligned}$$

The upper (lower) sign applies to

$$\begin{aligned} d_{i\perp} &> (<) d_{j\perp}, \\ \kappa(\vec{g}) &= [(2m/\hbar^2)(E_f + V_0 + i\Gamma) - (\vec{k}_0 + \vec{g})^2]^{1/2}, \end{aligned}$$

and

$$\vec{K}^\pm = (\vec{k}_0 + \vec{g}, \pm \kappa(\vec{g})).$$

$A$  is the area of the two-dimensional unit cell. The above series does, however, not converge in the case of the diagonal structure constants and instead the Ewald summation procedure has to be utilized.

With the definitions (B8) and (B9) the entire multiple scattering series for  $\Psi^1$  can be easily evaluated. In place of the single scattering term inside the large square brackets of Eq. (B5), we obtain

$$\begin{aligned} [\dots] &\rightarrow \left( \sum_{i=0}^{\infty} e^{-i k_{\perp} d_{i\perp}} t_i G_{i0} \right. \\ &\left. + \sum_{i,j=0}^{\infty} e^{-i k_{\perp} d_{i\perp}} t_i G_{ij} t_j G_{j0} + \dots \right)_{LL'}. \quad (\text{B11}) \end{aligned}$$

In the next step, we sum over all repeated scattering events within individual planes. This is accomplished by introducing the so-called single layer scattering matrices

$$\tau_i(E_f, \vec{k}_0) = t_i(\kappa) [1 - t_i(\kappa) G_{ii}(E_f, \vec{k}_0)]^{-1}. \quad (\text{B12})$$

The new series is the same as that in Eq. (B11) with  $t_i$  replaced by  $\tau_i$  and successive layer indices restricted to be unequal. It is then easily checked that this series can be conveniently expressed in terms of a set of multilayer scattering matrices  $T_{ij}(E_f, \vec{k}_0)$ , which are specified by the following system of equations:

$$T_{ij} = \tau_i \delta_{ij} + \sum_{k \neq i} \tau_i G_{ik} T_{kj}, \quad i, j, k = 0, 1, \dots \quad (\text{B13})$$

With these definitions, the final result for  $\Psi^1$  is given by

$$\begin{aligned} \Psi^2(\vec{R}) &= \frac{e^{i\kappa R}}{R} \sum_{L, L'} Y_{L'}^*(\hat{R}) \\ &\times \left( \sum_{i, j=0}^{\infty} e^{i k_{\perp} d_{i\perp}} T_{ij}(E_f, \vec{k}_{\parallel}) G_{j0}(E_f, \vec{k}_{\parallel}) \right)_{L'L} \\ &\times M_{L, L_i}(E_f, E_i). \end{aligned} \quad (\text{B14})$$

The sums over layer indices  $i, j$  are effectively limited to only a few terms because of the presence of damping.

The above result is derived under the assumption of translational invariance. If we allow the potential at the emitting site to differ from the remaining overlayer potentials due to the existence of the core hole, one is essentially confronted with a defect problem. To lowest order in the change of the  $t$  matrix at the origin,  $\delta t_0^i(k)$ , we have the following correction  $\Delta$  to the term inside the large parentheses of Eq. (B14):

$$\begin{aligned} \Delta_{LL'} &= \sum_{\vec{R}_0 \neq 0} \sum_{L''} \delta t_0^i(k) G_{LL''}(-\vec{R}_0) \\ &\times t_{\vec{R}_0}^{j''}(k) G_{L''L}(\vec{R}_0), \end{aligned} \quad (\text{B15})$$

where the sum over  $\vec{R}_0$  is over substrate as well as overlayer sites.

We conclude this appendix by pointing out that the solution of the system of equations in (B13) requires the inversion of a complex matrix with dimension  $N(l_{\max} + 1)^2$ , where  $N$  is the number of planes including the overlayer necessary to achieve convergence and  $l_{\max}$  is the highest phase shift considered. Since this matrix equation depends through the structure constant on the overlayer position relative to the substrate, the inversion would have to be performed whenever the adsorbate position is varied. This can, however, be avoided entirely by reformulating the multiple scattering series in Eq. (B11) in terms of substrate scattering matrices alone, which then do not need to be recalculated. This is accomplished by explicitly separating in Eq. (B11) scattering events that take place in the substrate from those that involve the overlayer. The final result is given in Appendix C. The same procedure can also be applied to derive the corresponding expressions for overlayer symmetries lower than  $(1 \times 1)$ . These results are also presented in Appendix C.

#### APPENDIX C

In this appendix we present an alternative expression for the multiple scattering series in Eqs.

(2.13), in order to allow for a computationally more practical variation of the overlayer position relative to the substrate. By summing first over scattering events in the substrate and subsequently over those in the adsorbate we obtain the following result:

$$\begin{aligned} \sum_{i, j=0}^{\infty} e^{-ik_{\perp} d_{i\perp}} T_{ij} G_{j0} &= \sum_{i, j=1}^{\infty} e^{-ik_{\perp} d_{i\perp}} T_{ij}^s G_{j0} \\ &+ \left( 1 + \sum_{i, j=1}^{\infty} e^{-ik_{\perp} d_{i\perp}} T_{ij}^s G_{j0} \right) (1 - \tau_0 g)^{-1} \tau_0 (G_{00} + g), \end{aligned} \quad (\text{C1})$$

where

$$g(E, \vec{k}_{\parallel}) = \sum_{i, j=1}^{\infty} G_{0i}(E, \vec{k}_{\parallel}) T_{ij}(E, \vec{k}_{\parallel}) G_{j0}(E, \vec{k}_{\parallel}) \quad (\text{C2})$$

and the  $T_{ij}^s$  are the substrate scattering matrices defined by the following system of equations:

$$T_{ij}^s = \tau_i \delta_{ij} + \sum_{k \neq i} \tau_i G_{ik} T_{kj}^s, \quad i, j, k = 1, 2, \dots \quad (\text{C3})$$

That Eq. (C1) is indeed an identity is easily verified by expanding each series and regrouping the individual contributions. The matrices in Eq. (C3) do not depend on the adsorbate and thus do not need to be recalculated if the overlayer position is changed. Only the structure constants  $G_{i0}$  and  $G_{0i}$ ,  $i = 1, 2, \dots$ , are affected. The dimension of the matrix to be inverted is now reduced to  $(N - 1)(l_{\max} + 1)^2$ ,  $N - 1$  being the number of substrate layers necessary for convergence.

Since the above outlined procedure completely separates the overlayer geometry from that of the underlying substrate, it can also be applied to adsorbates with symmetry other than  $(1 \times 1)$ .<sup>21</sup> The lowest-order term in Eq. (C1) in which the difference in planar symmetry becomes crucial is

$$\begin{aligned} \sum_{i=1}^{\infty} e^{-ik_{\perp} d_{i\perp}} \sum_{\vec{P}_A} e^{-i\vec{k}_{\parallel} \cdot \vec{P}_A} t_0 \sum_{\vec{P}} G(\vec{P}_A - \vec{P} - \vec{d}_i) t_i G(\vec{P} + \vec{d}_i) \\ \equiv \sum_{i=1}^{\infty} e^{-ik_{\perp} d_{i\perp}} t_0 \sum_{\vec{P}_A} e^{-i\vec{k}_{\parallel} \cdot \vec{P}_A} f(\vec{P}_A), \end{aligned} \quad (\text{C4})$$

where  $\vec{P} + \vec{d}_i$  denotes a site within the  $i$ th substrate plane and  $\vec{P}_A$  are the new set of adsorbate sites. Defining

$$f(\vec{k}_{\parallel}) = \sum_{\vec{P}} e^{-i\vec{k}_{\parallel} \cdot \vec{P}} f(\vec{P}), \quad (\text{C5})$$

we can express  $f(\vec{P})$  as follows:

$$f(\vec{P}) = (2\pi)^{-2} \int_{\text{BZ}} d^2 k' e^{i\vec{k}'_{\parallel} \cdot \vec{P}} f(\vec{k}'_{\parallel}). \quad (\text{C6})$$

Thus

$$\begin{aligned} \sum_{\vec{P}_A} e^{-i\vec{k}_{\parallel} \cdot \vec{P}_A} f(\vec{P}_A) &= (2\pi)^{-2} \int d^2 k' f(\vec{k}'_{\parallel}) \sum_{\vec{P}_A} e^{i(\vec{k}'_{\parallel} - \vec{k}_{\parallel}) \cdot \vec{P}_A} \\ &= c \left( f(\vec{k}_{\parallel}) + \sum_{\vec{g}_A} f(\vec{k}_{\parallel} + \vec{g}_A) \right), \end{aligned} \quad (\text{C7})$$

where  $c$  is the coverage and  $\vec{g}_A$  are the new reciprocal-lattice vectors of the superlattice. The higher-order terms in Eq. (C1) can be evaluated analogously with the result that the quantity  $g(\vec{k})$  is replaced by

$$g(E, \vec{k}_\parallel) - c \left( g(E, \vec{k}_\parallel) + \sum_{\vec{g}_A} g(E, \vec{k}_\parallel + \vec{g}_A) \right), \quad (\text{C8})$$

i. e., all structure constants remain unchanged with the exception of course of  $G_{00}(\vec{k})$  which now involves a sum over sites  $\vec{P}_A$  rather than  $\vec{P}$ . Therefore, in going from  $(1 \times 1)$  to other overlayer symmetries, the substrate scattering matrix has to be calculated at  $\vec{k}_\parallel$  and  $\vec{k}_\parallel + \vec{g}_A$ , an additional computational effort that scales proportionally with the inverse of the coverage (rather than  $c^{-3}$  as in the sublattice formalism).

\*Research supported by the Laboratory for Research on the Structure of Matter and the Advanced Research Projects Agency of the Department of Defense as monitored by the Air Force Office of Scientific Research under Contract No. F44620-75-C-0069 and the NSF under Grants DMR 2-03025 and 73-07682.

<sup>1</sup>A. Liebsch, Phys. Rev. Lett. 32, 1203 (1974).

<sup>2</sup>J. W. Gadzuk, Solid State Commun. 15, 1011 (1974); Phys. Rev. B 10, 5030 (1974).

<sup>3</sup>W. E. Spicer, in Optical Properties of Solids—New Developments, edited by B. O. Seraphin (North-Holland, Amsterdam, 1975) (to be published); D. Menzel, J. Vac. Sci. Technol. 12, 313 (1975); C. R. Brundle, *ibid.* 11, 212 (1974); D. E. Eastman and J. E. Demuth; Jpn. J. Appl. Phys. Suppl. 2, 827 (1974); E. W. Plummer, in *Topics in Applied Physics*, edited by R. Gomer (Springer, New York, 1975), Vol. 5; A. M. Bradshaw, L. Cederbaum, and W. Domcke, in *Electron Spectroscopy* (Springer, Heidelberg, 1975), Vol. 24.

<sup>4</sup>B. J. Waclawski, T. V. Vorburger, and R. J. Stein, J. Vac. Sci. Technol. 12, 301 (1975); W. F. Egelhoff and D. L. Perry, Phys. Rev. Lett. 34, 93 (1975); J. Anderson and G. J. Lapeyre, Bull. Am. Phys. Soc. 20, 304 (1975).

<sup>5</sup>D. E. Sayers, F. W. Lytle, and E. A. Stern, in *Advances in x-ray Analysis*, edited by B. L. Henke, J. B. Newkirk, and G. R. Mallett (Plenum, New York, 1970), Vol. 13, p. 248; E. A. Stern, Phys. Rev. B 10, 3027 (1974); C. A. Ashley and S. Doniach, *ibid.* 11, 1279 (1975); P. A. Lee and J. B. Pendry, *ibid.* 11, 2795 (1975).

<sup>6</sup>T. Matsudaira, M. Watanabe, and M. Onchi, Jpn. J. Appl. Phys. Suppl. 2, 181 (1974); L. McDonnell, D. P. Woodruff, and B. W. Holland, Surf. Sci. (to be published); D. M. Zehner, J. R. Noonan, L. H. Jenkins, and T. Kaplan, Bull. Am. Phys. Soc. 20, 357 (1975).

<sup>7</sup>A. Liebsch (unpublished).

<sup>8</sup>P. J. Feibelman, Phys. Rev. Lett. 34, 1092 (1975); K. L. Kliewer, *ibid.* 33, 900 (1974).

<sup>9</sup>J. B. Pendry, *Low Energy Electron Diffraction* (Academic, New York, 1974), p. 119. This reference discusses the same phenomenon in the case of LEED.

<sup>10</sup>J. E. Demuth, D. W. Jepsen, and P. M. Marcus, Phys. Rev. Lett. 31, 540 (1973); C. B. Duke, N. O. Lipari, and G. E. Laramore, J. Vac. Sci. Technol. 12, 222 (1975).

<sup>11</sup>C. B. Duke, in *Dynamic Aspects of Surface Physics*, edited by F. O. Goodman (Editrice Compositori, Bologna, 1974), p. 99; D. W. Jepsen, P. M. Marcus, and F. Jona, Phys. Rev. B 5, 3933 (1972); J. B. Pendry, see Ref. 8.

<sup>12</sup>C. B. Duke and C. W. Tucker, Jr., Phys. Rev. Lett. 23, 1163 (1969).

<sup>13</sup>C. Caroli, D. Lederer-Rozenblatt, B. Roulet, and D. Saint-James, Phys. Rev. B 8, 4552 (1973); G. D. Mahan, *ibid.* 2, 4334 (1970); W. I. Schaich and N. W. Ashcroft, *ibid.* 3, 2452 (1971); P. J. Feibelman and D. E. Eastman, *ibid.* 10, 4932 (1974).

<sup>14</sup>H. A. Bethe and E. E. Salpeter, *Quantum Mechanics of One and Two Electron Atoms* (Academic, New York, 1957), see especially Eqs. (59.5) and (69.5); J. Cooper and R. N. Zare, *Lectures in Theoretical Physics*, (Gordon and Breach, New York, 1969), Vol. XI C, p. 317; D. Dill and J. L. Dehmer, J. Chem. Phys. 61, 692 (1974).

<sup>15</sup>C. Caroli *et al.*, Ref. 13; and P. J. Feibelman, Surf. Sci. 46, 558 (1974).

<sup>16</sup>T. Gustafsson and E. W. Plummer (unpublished).

<sup>17</sup>See Ref. 8, p. 168.

<sup>18</sup>G. E. Laramore, C. B. Duke, and N. O. Lipari (unpublished); Ref. 8, p. 245.

<sup>19</sup>A. Liebsch and E. W. Plummer, Discuss. Faraday Soc. 58, 19 (1975).

<sup>20</sup>J. E. Beeby, J. Phys. C 1, 82 (1963).

<sup>21</sup>A. Liebsch, J. Vac. Sci. Technol. 11, 201 (1974).